arXiv:1701.03910v1 [astro-ph.IM] 14 Jan 2017

Mean transverse momentum as a mass composition estimator of cosmic rays

H. Hedayati Kh.
email hedayati@kntu.ac.ir

Department of Physics, K.N. Toosi University of Technology,
P.O. Box 15875-4416, Tehran, Iran

January 2017

Abstract

Determination of mass composition of high energy cosmic rays is one of the greatest challenge in modern astrophysics. All of previous methods for finding the mass composition of primary cosmic rays in a surface array at least require two independent measurements (e.g. muon and electron components) of extensive air showers (EAS). Here a new statistical parameter is introduced which can be used to determine the mass composition of vertical downward cosmic rays in a simple surface array. The most interesting thing about the new parameter is that it does not need two independent measurements and can be used in a simple surface array which does not have muon detectors.

Keywords— Cosmic ray; Extensive air showers; Mass compositions

1 Introduction

From the beginning of cosmic ray researches, one of the most important questions about them had been about their nature. After it became clear that most of them are ionized nucleus of common atoms , this question was changed to a question of frequency of individual nucleus in the primary cosmic rays composition. Now, the mass composition of primary cosmic rays is very important for the interpretation of different astrophysical processes and for acceleration mechanisms of ultra high energy cosmic rays.
Up to energies of about 10^{14} eV, balloon-borne or satellite-borne experiments directly measured the mass composition of primaries with negligible uncertainties [11, 7]. At higher energies, direct measurement of mass composition is not possible and mass composition estimation is only possible through extensive air showers which is generated by primary cosmic rays. Propagation of an extensive air shower through atmosphere includes lots of intrinsic fluctuations and so ground based experiments can not access the mass composition of every single primary.
Strictly speaking, no EAS experiment measures the mass content of primaries. Instead, they measure one or more of primaries mass sensitive parameters of extensive air showers. The events can then be interpreted in terms of primary mass by a comparison to air shower simulations using different hadronic interaction models. Mass composition estimation of primaries (MCEP) can be achieved either in observation of longitudinal development of EAS through atmosphere or simultaneous measurement of the electromagnetic and muonic component of EASs in a surface array. Where, in the former case, people usually determine the EAS maximum development through atmosphere which is a relatively good mass sensitive parameter.
From the EAS maximum development measurements, two observables are derived: $< X_{max} >$, the mean depth of EAS maximum development in g/cm^2 and its standard deviation, $\sigma(X_{max})$, which are related to $\ln A$ and $\sigma(\ln A)$, where A is the atomic mass of the primary. EAS simulations shows that proton and iron induced EASs maximum development are expected to differ by around 100 g/cm^2 . However, unfortunately even extreme mass content like proton and iron have considerable overlap [21]. Currently, direct observation of the EAS maximum development is only possible by fluorescence light telescopes. At the moment, there are two active experiments that use fluorescence telescopes for MCEP: The Pierre Auger observatory [1] and the Telescope Array (TA) [22]. For the Auger Observatory, EAS maximum depth is determined with a resolution of about 25 g/cm^2 at low energies decreasing down to about 15 g/cm^2 above 10^18 eV. For the latter, the resolution is better than 40 g/cm^2 at energy of 10^16 eV and at higher energies, the accuracy

performs better and reaches to 20 g/cm^2 [25].
Also, non-imaging Cherenkov Telescope can be used for determination of the EAS maximum. They can deduce it either from the measurement of the pulse width at 400 m from the core and from the ratio of the photon densities at two different distances from the shower core [24].
Recently, the Low Frequency Array, LOFAR [27], a radio telescope consisting of thousands of crossed dipoles, reported a radio measurements of EAS maximum with a high resolution, a mean uncertainty of 16 grams per square centimeter [9]. The situation will be even better with the new installations in progress. For example, for the Square Kilometre Array (SKA) which will be operational in Australia in 2023, it claims that it will reach to a resolution of 6 g/cm^2 in determination of EAS maximum [20]. If that is the case, this results in a better mass spectroscopy than ever done before. Although with such a high resolution in determination of X_{max}, a far better mass spectroscopy is possible, single event mass determination is nevertheless impossible.
Another method for the MCEP is the measurement of particle densities at a surface array. Unlike the observation of EAS maximum development which takes places in a wide range of Earth's atmosphere, surface arrays measure EAS profile only in a single plane and so is more susceptible to the EAS fluctuations. Nevertheless, surface arrays are far more common than telescopes, air Cherenkov detectors and recently developed radio detection techniques. Furthermore, unlike telescopes or air Cherenkov detectors, they have a full duty cycle. So MCEP in surface arrays are still widely used.
The most common method for the MCEP in a surface array is the estimation of electron and muon numbers. While the sum of electron and muon numbers at the ground relate to the energy content of an EAS, the ratio of muon number to electron number is an indication of the primary mass content. The most widely used technique for electron-muon discrimination in a surface array is simultaneous use of unshielded and shielded scintillation detectors (e.g. AGASA [12], CASA-MIA [8], EAS-TOP [4], GRAPES [18], KASCADE [5], KASCADE-Grande [6], Maket-ANI [14], GAMMA [16], and Yakutsk [3]). The Auger observatory uses Cherenkov tanks which also enables a limited muon identification [2].
More recently, Canal et al. in their simulations found that the ratio r_{me} of the muon to the electromagnetic component of an EAS at the ground level is a good measure for the MCEP. They reported that the value of r_{me} enable us to reach a 98% efficiency for discrimination of proton from iron primaries [10].
Another method for the MCEP is the analysis of lateral distribution of charged particles of EASs. Most of lateral distribution functions (LDF) which are in use for energy estimation of EASs have an age parameter which is an

estimation of EASs maximum development depth. EASs of heavy primaries reach their maximum development depth at higher altitudes than EASs of lighter primaries. So the LDF of heavier primaries are flatter and age parameter has higher values than lighter primaries. However, the precision of this method for the the MCEP is lower than other methods (for a review of MCEP methods, see [21]).
In this paper, a new parameter is introduced which enable a good MCEP for vertical EASs. This parameter can be used in a simple surface array that lacks muon detectors and only measures charged particles in general.

2 Mean transverse momentom as a mass composition estimator

From the new results of LHC, it is evident that the more multiplicity of secondary particles of a reaction, the higher mean transverse momentum per particle of the reactions products (e.g. see [13]). Actually, transverse momentum per particle has a direct relationship with multiplicity.
On the other hand, we conclude from extensive simulations of EASs which conducted by different research groups that the higher the mass composition of primaries, the higher the multiplicity of secondary particles (see chapter 3 of [17]).
The overall result of the above discussion is that when the primary particle is heavier, the generated secondary particles by it have higher transverse momentum. So if we could determine the mean transverse momentum per particles ($\langle P_T \rangle$) of secondary particles of an EASs, we would enable to determine their rough mass composition.
In order to test this hypothesis, some CORSIKA [19] simulated EASs have been generated whose general properties are summarized in table 1. The primary particles of these EASs are protons or irons. For each type and energy, 10000 EASs have been separately generated (e.g. 10000 EASs whose primary particles are iron and primary energies is 200 TeV are generated). According to table 1, there are 6 different combinations of types and energies altogether. So the number of all generated EASs are 60000.

For the vertical EASs, $\langle P_T \rangle$ is calculated from the following equation:

$$\langle P_T \rangle = \frac{1}{N} \sum_{i=1}^{N} \sqrt{p_{xi}^2 + p_{yi}^2} \tag{1}$$

where p_{xi} and p_{yi} are the components of horizontal momentum of secondary particles.

Specifications	Values
energy of primaries	$E = 100$, 200 and 300 TeV
type of primaries	proton and iron
zenith angle of primaries	$\theta = 0^\circ$
geographical longitude	51 E
geographical latitude	35 N
altitude	1200 m
earth magnetic field (B_x)	$28.1\,\mu$T
earth magnetic field (B_z)	$38.4\,\mu$T
low energy hadronic model	Fluka 2011.2b [15]
high energy hadronic model	QGSJETII-04 [23]

Table 1: EASs' specifications. Other specifications are CORSIKA default values.

Figure 1 shows the distribution of the $\langle P_T \rangle$ for 20000 EASs of table 1 (10000 proton initiated EASs and 10000 iron initiated EASs) on the ground level. As can be seen in this figure, iron primaries are completely distinguished from protons based on their charged secondary particles' $\langle P_T \rangle$s. Actually $\langle P_T \rangle$ of iron EASs are higher than proton EASs which is in consistency with the above points. Also, as is evident from this figure, there is no difference between electronic and muonic components in this behavior, regardless of some few iron EASs with low $\langle P_T \rangle$ electrons. These exceptional cases occurs when most energy of the EASs is transferred to the muonic component and a very low fraction of energy remains for the electronic component. These EASs are not often detectable by the surface arrays.

3 Mean transverse distance from axis

Although, $\langle P_T \rangle$ is a useful parameter for the MCEP, it can not be directly obtained by the current surface arrays in use (A surface array of hodoscopes is probably appropriate for this purpose). So we should find a new parameter which has some relation with $\langle P_T \rangle$ and can be obtained from the information provided by a common surface array.
Although the propagation of an EAS in the atmosphere has lots of stochastic fluctuations, obviously when the $\langle P_T \rangle$ of an EAS is large, its secondary particles have a higher chance to be found at larger distances from axis. So a new quantity of an EAS which can be a measure of its $\langle P_T \rangle$ is the mean

transverse distance of particles from the axis ($\langle d_T \rangle$):

$$\langle d_T \rangle = \frac{1}{N} \sum_{i=1}^{N} d_i, \tag{2}$$

where d_i is the distance of ith secondary particle from the axis.

Figure 2 shows the distribution of $\langle d_T \rangle$ for the same showers as figure 1. It is apparent from this figure that $\langle d_T \rangle$ is a suitable parameter for the MCEP, as it was anticipated. However, distribution of $\langle d_T \rangle$ for electrons is better discriminated than for muons. It may be contributed to the propagation of low energy muons in atmosphere. Also, it is evident that $\langle d_T \rangle$ of all charged particles of EASs is again a relatively appropriate parameter for the MCEP.

4 An investigation of the relationship of mean transverse distance from axis and energy

As we saw in the previous sections, it seems that $\langle P_T \rangle$ (and consequently $\langle d_T \rangle$) is a useful parameter for the MCEP. However, if it has a complicated relationship with the energy of the primary, its use for the MCEP purposes will be very limited.

Figure 3 shows the probability density of $\langle P_T \rangle$ for all EASs of table 1. As can be seen from this figure, for all three energies shown, $\langle P_T \rangle$ is well-separated for proton and iron primaries. Another interesting thing in this figure is that it seems that the distribution of $\langle P_T \rangle$ becomes sharper with increasing energy of the primaries (especially for the irons). Also the $\langle P_T \rangle$ approaches to lower (but distinct values for irons from protons).

Figure 4 shows the the probability density of $\langle d_T \rangle$ for all EASs of table 1. Again, for the electronic component the separation is better than muonic component.

When this paper was at final stages of writing, a new paper was published [26] which is reported a new parameter like $\langle d_T \rangle$ and shows that it has a universality for all EASs. So it seems that $\langle d_T \rangle$ can be applied for non vertical EASs and also is model-independent.

5 Conclusions

In this paper a new parameter has been introduced which can be applied for the mass composition estimation of primary cosmic rays. This parameter is the mean transverse momentum per particles of the secondary particles of

an EAS, $\langle P_T \rangle$. It is also shown that a related parameter to $\langle P_T \rangle$ which can be directly measured is the mean transverse distance from axis, $\langle d_T \rangle$.
Although $\langle d_T \rangle$ is good enough for discrimination of iron primaries from proton primaries in the electronic component of an EAS, it is not so good in muonic component. It is also shown that the distributions of these parameters are sharper in higher energies.

References

[1] J Abraham, P Abreu, M Aglietta, C Aguirre, EJ Ahn, D Allard, I Allekotte, J Allen, P Allison, J Alvarez-Muniz, et al. The fluorescence detector of the pierre auger observatory. *Nuclear Instruments and Methods in Physics Research Section A: Accelerators, Spectrometers, Detectors and Associated Equipment*, 620(2):227–251, 2010.

[2] J. Abraham, M. Aglietta, I.C. Aguirre, M. Albrow, D. Allard, I. Allekotte, P. Allison, J. Alvarez Muiz, M.G. do Amaral, M. Ambrosio, L. Anchordoqui, R. Andrews, M. Anguiano, J.C. dos Anjos, C. Aramo, S. Argiro, K. Arisaka, J.C. Arteaga, S. Atulugama, M. Ave, G. Avila, R. Baggio, X. Bai, A.F. Barbosa, H.M.J. Barbosa, D. Barnhill, S.L.C. Barroso, P. Bauleo, J. Beatty, T. Beau, K.-H. Becker, J.A. Bellido, P. Bello, T. Bergmann, E. Berman, X. Bertou, P. Biermann, P. Billoir, R. Biral, H. Bluemer, M. Bohacova, E. Bollmann, C. Bonifazi, M. Boratav, A. Boselli, J. Brack, J.-M. Brunet, H. Bui-Duc, V. Cabrera, D.V. Camin, J.-N. Capdevielle, A. Carreo, N. Cartiglia, R. Caruso, L.A. de Carvalho, S. Casanova, E. Casimiro, A. Castellina, J. Castro, P.W. Cattaneo, L. Cazon, R. Cester, N. Chvez, D. Cheam, A. Chiavassa, J.A. Chinellato, M. Chiosso, A. Chou, J. Chye, A. Cillis, B. Civit, D. Claes, P.D.J. Clark, R.W. Clay, F. Cohen, A. Cordero, A. Cordier, E. Cormier, J. Cotzomi, U. Cotti, S. Coutu, C.E. Covault, A. Creusot, J.W. Cronin, M. Cuautle, S. Dagoret-Campagne, T. Dang-Quang, P. Da Silva, J. Darling, P. Darriulat, K. Daumiller, B.R. Dawson, L. de Bruijn, A. De Capoa, M.A.L. de Oliveira, V. de Souza, A. Della Selva, O. Deligny, J.C. Diaz, C. Dobrigkeit, J.C. D'Olivo, A. Dorofeev, M.T. Dova, A. Dye, M.A. DuVernois, R. Engel, L.N. Epele, P. Eschstruth, C.O. Escobar, A. Etchegoyen, P. Facal San Luis, A.C. Fauth, N. Fazzini, A. Fernndez, A.M.J. Ferrero, B. Fick, A. Filevich, A. Filipi, R. Fonte, W. Fulgione, E. Gmez, B. Garcia, C.A. Garcia, H. Geenen, H. Gemmeke, C. Germain-Renaud, P.L. Ghia, K. Gibbs, M. Giller, J. Gitto, H. Glass, M. Gmez Berisso, P.F. Gomez Vitale,

J. Gonzlez, J. Gonzlez, D. Gora, A. Goodwin, P. Gouffon, V. Grassi, A.F. Grillo, C. Grunfeld, J. Grygar, F. Guarino, G. Guedes, C. Guerard, R. Gumbsheimer, J.L. Harton, F. Hasenbalg, D. Heck, J.M. Hernndez, D. Hoffer, C. Hojvat, P. Homola, M. Horvat, M. Hrabovsky, A. Insolia, S. Jaminion, Y. Jernimo, L. Jiang, M. Kaducak, K.-H. Kampert, B. Keilhauer, E. Kemp, H. Klages, M. Kleifges, J. Kleinfeller, J. Knapp, A. Kopmann, N. Kunka, M. Kutschera, C. Lachaud, M. Lapolla, A. Letessier-Selvon, I. Lhenry-Yvon, J. Lloyd-Evans, R. Lpez, A. Lopez Aguera, M. Lucano, R. Luna, Y. Ma, M.E. Manceido, P.F. Manfredi, L. Manhaes, P. Mantsch, A.G. Mariazzi, M.J. Markus, G. Martin, O. Martineau, J. Martinez, N. Martinez, O. Martnez, H.-J. Mathes, J.A.J. Matthews, J. Matthews, G. Matthiae, E. Marques, P. Matussek, G. Maurin, D. Maurizio, P. Mazur, T. McCauley, M. McEwen, R.R. McNeil, C. Medina, M.C. Medina, G. Medina-Tanco, D. Melo, M. Melocchi, E. Menichetti, A. Menshikov, F. Meyer, R. Meyhandan, J.C. Meza, G. Miele, W. Miller, M. Mohammed, D. Monnier-Ragaigne, C. Morello, E. Moreno, M. Mostafa, R. Mussa, H. Nassini, G. Navarra, L. Nellen, F. Nerling, C. Newman-Holmes, D. Nicotra, S. Nigro, D. Nitz, H. Nogima, D. Nosek, M. Nuez, T. Ohnuki, A. Olinto, S. Ostaptchenko, M. Palatka, G. Parente, E. Parizot, E.H. Pasaye, N. Pastrone, M. Patel, T. Paul, I. Pedraza, J. Pekala, R. Pelayo, I.M. Pepe, A. Prez-Lorenzana, L. Perrone, N. Peshman, S. Petrera, P. Petrinca, D. Pham-Ngoc, P. Pham-Trung, T. Pierog, O. Pisanti, N. Playez, E. Ponce, T.A. Porter, L. Prado Junior, P. Privitera, M. Prouza, C.L. Pryke, J.B. Rafert, G. Raia, S. Ranchon, L. Ratti, D. Ravignani, V. Re, H.C. Reis, S. Reucroft, B. Revenue, M. Richter, J. Ridky, A. Risi, M. Risse, V. Rizi, M.D. Roberts, C. Robledo, G. Rodriguez, J. Rodriquez, J. Rodriquez Martino, S. Romn, L. Rosa, M. Roth, A.C. Rovero, H. Salazar, G. Salina, F. Sanchez, M. Santander, L.G. dos Santos, R. Sato, P. Schovanek, V. Scherini, S.J. Sciutto, G. Sequeiros-Haddad, R.C. Shellard, E. Shibuya, F.V. Siguas, W. Slater, N. Smetniansky-De Grande, K. Smith, G.R. Snow, P. Sommers, C. Song, H. Spinka, F. Suarez, T. Suomijrvi, D. Supanitsky, J. Swain, Z. Szadkowski, A. Tamashiro, G.J. Thornton, T. Thouw, R. Ticona, W. Tkaczyk, C.J. Todero Peixoto, A. Tripathi, G. Tristram, M. Trombley, D. Tscherniakhovski, P. Tuckey, V. Tunnicliffe, M. Urban, C. Uribe Estrada, J.F. Valds, A. Vargas, C. Vargas, R. Vazquez, D. Veberi, A. Veiga, A. Velarde, F. Vernotte, V. Verzi, M. Videla, C. Vigorito, L.M. Villaseor, M. Vlcek, L. Voyvodic, T. Vo-Van, T. Waldenmaier, P. Walker, D. Warner, A.A. Watson, Ch. Wiebusch, G. Wieczorek, B. Wilczynska, H. Wilczynski, N.R. Wild, T. Yamamoto, E. Zas, D. Zavrtanik, M. Za-

vrtanik, A. Zepeda, C. Zhang, and Q. Zhu. Properties and performance of the prototype instrument for the pierre auger observatory. *Nuclear Instruments and Methods in Physics Research Section A: Accelerators, Spectrometers, Detectors and Associated Equipment*, 523(12):50 – 95, 2004.

[3] B. N. Afanasiev and *et al.* [Yakutsk Collaboration]. Proceedings of the tokyo workshop on techniques for the study of the extremely high energy cosmic rays. page 35, 1993.

[4] M. Aglietta, B. Alessandro, P. Antonioli, F. Arneodo, L. Bergamasco, A. Campos Fauth, C. Castagnoli, A. Castellina, C. Cattadori, A. Chiavassa, G. Cini, B. D'Ettorre Piazzoli, G. Di Sciascio, W. Fulgione, P. Galeotti, P.L. Ghia, M. Iacovacci, G. Mannocchi, C. Morello, G. Navarra, L. Riccati, O. Saavedra, G.C. Trinchero, P. Vallania, and S. Vernetto. Uhe cosmic ray event reconstruction by the electromagnetic detector of eas-top. *Nuclear Inst. and Methods in Physics Research, A*, 336(1-2):310–321, 1993. cited By 70.

[5] T. Antoni, W.D. Apel, F. Badea, K. Bekk, A. Bercuci, H. Blmer, H. Bozdog, I.M. Brancus, C. Bttner, A. Chilingarian, K. Daumiller, P. Doll, J. Engler, F. Feler, H.J. Gils, R. Glasstetter, R. Haeusler, A. Haungs, D. Heck, J.R. Hrandel, A. Iwan, K.-H. Kampert, H.O. Klages, G. Maier, H.J. Mathes, H.J. Mayer, J. Milke, M. Mller, R. Obenland, J. Oehlschlger, S. Ostapchenko, M. Petcu, H. Rebel, M. Risse, M. Roth, G. Schatz, H. Schieler, J. Scholz, T. Thouw, H. Ulrich, A. Vardanyan, J. Weber, A. Weindl, J. Wentz, J. Wochele, J. Zabierowski, and S. Zagromski. The cosmic-ray experiment kascade. *Nuclear Instruments and Methods in Physics Research, Section A: Accelerators, Spectrometers, Detectors and Associated Equipment*, 513(3):490–510, 2003. cited By 200.

[6] W.D. Apel, J.C. Arteaga, A.F. Badea, K. Bekk, M. Bertaina, J. Blmer, H. Bozdog, I.M. Brancus, P. Buchholz, E. Cantoni, A. Chiavassa, F. Cossavella, K. Daumiller, V. De Souza, F. Di Pierro, P. Doll, R. Engel, J. Engler, M. Finger, D. Fuhrmann, P.L. Ghia, H.J. Gils, R. Glasstetter, C. Grupen, A. Haungs, D. Heck, J.R. Hrandel, T. Huege, P.G. Isar, K.-H. Kampert, D. Kang, D. Kickelbick, H.O. Klages, K. Link, P. Uczak, M. Ludwig, H.J. Mathes, H.J. Mayer, M. Melissas, J. Milke, B. Mitrica, C. Morello, G. Navarra, S. Nehls, J. Oehlschlger, S. Ostapchenko, S. Over, N. Palmieri, M. Petcu, T. Pierog, H. Rebel, M. Roth, H. Schieler, F. Schrder, O. Sima, M. Stmpert, G. Toma, G.C. Trinchero,

H. Ulrich, A. Weindl, J. Wochele, M. Wommer, and J. Zabierowski. The kascade-grande experiment. *Nuclear Instruments and Methods in Physics Research, Section A: Accelerators, Spectrometers, Detectors and Associated Equipment*, 620(2-3):202–216, 2010. cited By 93.

[7] Mirko Boezio and Emiliano Mocchiutti. Chemical composition of galactic cosmic rays with space experiments. *Astroparticle Physics*, 3940:95 – 108, 2012. Cosmic Rays Topical Issue.

[8] A. Borione, C.E. Covault, J.W. Cronin, B.E. Fick, K.G. Gibbs, H.A. Krimm, N.C. Mascarenhas, T.A. McKay, D. Mller, B.J. Newport, R.A. Ong, L.J. Rosenberg, H. Sanders, M. Catanese, D. Ciampa, K.D. Green, J. Kolodziejczak, J. Matthews, D. Nitz, D. Sinclair, and J.C. van der Velde. A large air shower array to search for astrophysical sources emitting -rays with energies 1014 ev. *Nuclear Inst. and Methods in Physics Research, A*, 346(1-2):329–352, 1994. cited By 69.

[9] S Buitink, A Corstanje, H Falcke, JR Hörandel, T Huege, A Nelles, JP Rachen, L Rossetto, P Schellart, O Scholten, et al. A large light-mass component of cosmic rays at 1017–1017.5 electronvolts from radio observations. *Nature*, 531(7592):70–73, 2016.

[10] CA García Canal, JI Illana, M Masip, and SJ Sciutto. A new observable in extensive air showers. *Astroparticle Physics*, 2016.

[11] Antonella Castellina and Fiorenza Donato. Astrophysics of galactic charged cosmic rays. *Planets, Stars and Stellar Systems: Volume 5: Galactic Structure and Stellar Populations*, pages 725–788, 2013.

[12] N. Chiba, K. Hashimoto, N. Hayashida, K. Honda, M. Honda, N. Inoue, F. Kakimoto, K. Kamata, S. Kawaguchi, N. Kawasumi, Y. Matsubara, K. Murakami, M. Nagano, S. Ogio, H. Ohoka, To. Saito, Y. Sakuma, I. Tsushima, M. Teshima, T. Umezawa, S. Yoshida, and H. Yoshii. Akeno giant air shower array (agasa) covering 100 km2 area. *Nuclear Inst. and Methods in Physics Research, A*, 311(1-2):338–349, 1992. cited By 95.

[13] ALICE collaboration et al. Multiplicity dependence of the average transverse momentum in pp, p–pb, and pb–pb collisions at the lhc. *Physics Letters B*, 727(4):371–380, 2013.

[14] TV Danilova, EA Danilova, AB Ezlikin, NM Nikolskaia, SJ Nikolsky, VA Romachin, SA Slavatinsky, BV Subbotin, EJ Tukich, KM Avakian,

et al. The ani experiment: on the investigation of interactions from hadrons and nuclei in the energy range 103–105 tev. *Nuclear Instruments and Methods in Physics Research Section A: Accelerators, Spectrometers, Detectors and Associated Equipment*, 323(1-2):104–107, 1992.

[15] Alfredo Ferrari, Paola R Sala, Alberto Fasso, and Johannes Ranft. Fluka: A multi-particle transport code (program version 2005). Technical report, 2005.

[16] A.P. Garyaka, R.M. Martirosov, S.V. Ter-Antonyan, N. Nikolskaya, Y.A. Gallant, L. Jones, and J. Procureur. Rigidity-dependent cosmic ray energy spectra in the knee region obtained with the gamma experiment. *Astroparticle Physics*, 28(2):169–181, 2007. cited By 22.

[17] Peter Karl Grieder. *Extensive Air Showers*. Springer, 2010.

[18] S.K. Gupta, Y. Aikawa, N.V. Gopalakrishnan, Y. Hayashi, N. Ikeda, N. Ito, A. Jain, A.V. John, S. Karthikeyan, S. Kawakami, T. Matsuyama, D.K. Mohanty, P.K. Mohanty, S.D. Morris, T. Nonaka, A. Oshima, B.S. Rao, K.C. Ravindran, M. Sasano, K. Sivaprasad, B.V. Sreekantan, H. Tanaka, S.C. Tonwar, K. Viswanathan, and T. Yoshikoshi. Grapes-3 - a high-density air shower array for studies on the structure in the cosmic-ray energy spectrum near the knee. *Nuclear Instruments and Methods in Physics Research, Section A: Accelerators, Spectrometers, Detectors and Associated Equipment*, 540(2-3):311–323, 2005. cited By 39.

[19] Dieter Heck, G Schatz, J Knapp, T Thouw, and JN Capdevielle. Corsika: A monte carlo code to simulate extensive air showers. Technical report, 1998.

[20] Tim Huege, Justin D Bray, Stijn Buitink, David Butler, Richard Dallier, Ron D Ekers, Torsten Enßlin, Heino Falcke, Andreas Haungs, Clancy W James, et al. Ultimate precision in cosmic-ray radio detection—the ska. *arXiv preprint arXiv:1608.08869*, 2016.

[21] Karl-Heinz Kampert and Michael Unger. Measurements of the cosmic ray composition with air shower experiments. *Astroparticle Physics*, 35(10):660–678, 2012.

[22] JN Matthews, C Jui, Pierre Sokolsky, M Fukushima, G Thomson, H Sagawa, and S Ogio. The telescope array experiment. In *Institute of High Energy Physics*, 2011.

[23] Sergey Ostapchenko. Monte carlo treatment of hadronic interactions in enhanced pomeron scheme: Qgsjet-ii model. *Physical Review D*, 83(1):014018, 2011.

[24] VV Prosin, SF Berezhnev, NM Budnev, A Chiavassa, OA Chvalaev, OA Gress, AN Dyachok, SN Epimakhov, NI Karpov, NN Kalmykov, et al. Tunka-133: Results of 3 year operation. *Nuclear Instruments and Methods in Physics Research Section A: Accelerators, Spectrometers, Detectors and Associated Equipment*, 756:94–101, 2014.

[25] VV Prosin, NM Budnev, A Chiavassa, AN Dyachok, SN Epimakhov, F Fenu, Yu A Fomin, OA Gress, TI Gress, NN Kalmykov, et al. Results and perspectives of cosmic ray mass composition studies with eas arrays in the tunka valley. In *Journal of Physics: Conference Series*, volume 718, page 052031. IOP Publishing, 2016.

[26] R Raikin, T Serebryakova, A Lagutin, and N Volkov. Model-stable universality of the air shower electromagnetic component: an approach to solving the mass composition problem. *arXiv preprint arXiv:1612.01250*, 2016.

[27] MP Van Haarlem, MW Wise, AW Gunst, George Heald, JP McKean, JWT Hessels, AG De Bruyn, Ronald Nijboer, John Swinbank, Richard Fallows, et al. Lofar: The low-frequency array. *Astronomy & Astrophysics*, 556:A2, 2013.

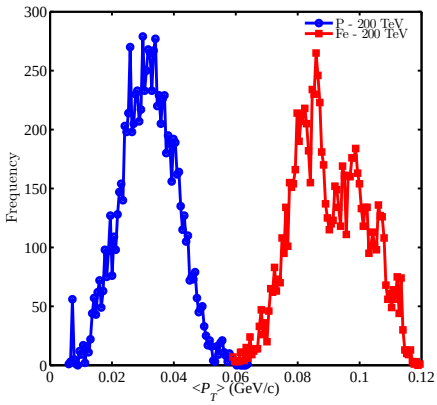

(a) $\langle P_T \rangle$ distribution for all charged particles.

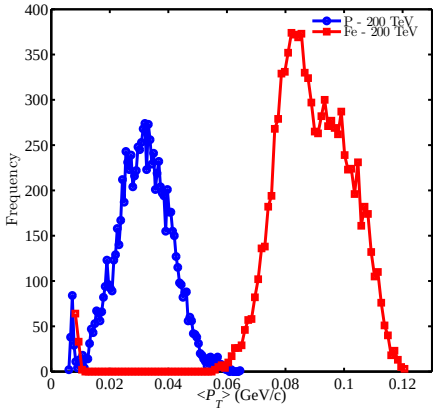

(b) $\langle P_T \rangle$ distribution for electrons and positrons.

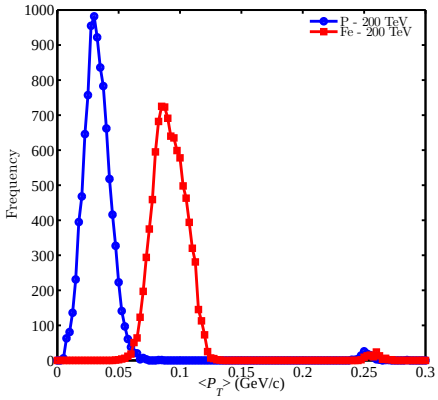

(c) $\langle P_T \rangle$ distribution for muons.

Figure 1: The frequency curves represents the $\langle P_T \rangle$ for secondary particles of vertical simulated EASs. The energies of all primaries are 200 TeV. Blue lines belongs to proton initiated EASs and red lines belongs to iron primaries.

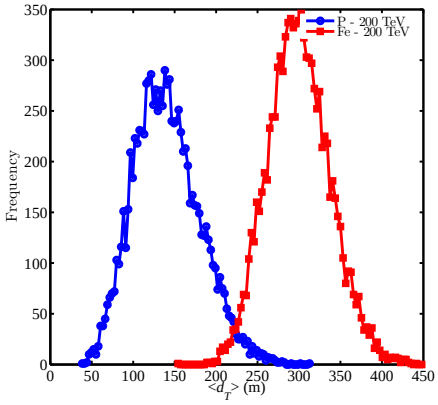

(a) $\langle d_T \rangle$ distribution for all charged particles.

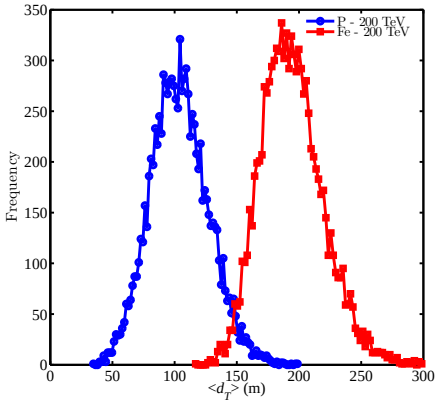

(b) $\langle d_T \rangle$ distribution for electrons and positrons.

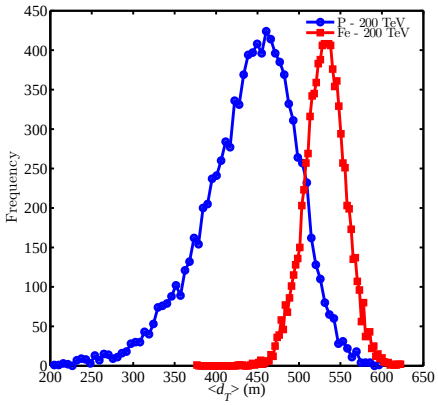

(c) $\langle d_T \rangle$ distribution for muons.

Figure 2: The frequency curves of $\langle d_T \rangle$. The applied EASs are the same as the previous figure.

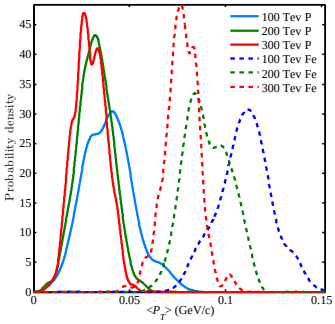

(a) $\langle P_T \rangle$ for all charged particles.

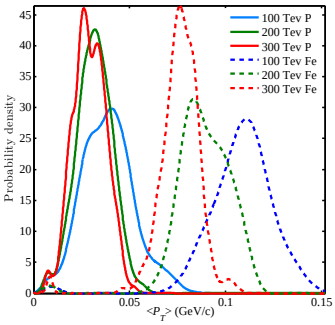

(b) $\langle P_T \rangle$ for electrons and positrons.

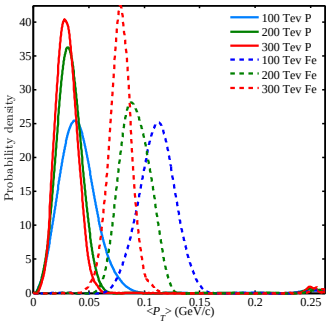

(c) $\langle P_T \rangle$ for muons.

Figure 3: The probability density of $\langle P_T \rangle$. The properties of the applied EASs are shown in the legends as before.

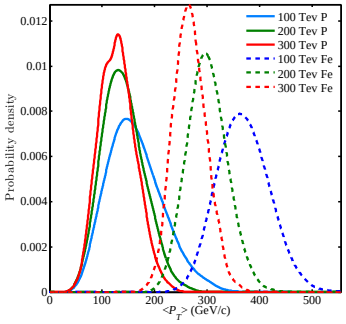

(a) $\langle d_T \rangle$ for all charged particles.

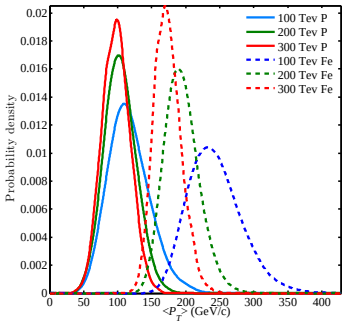

(b) $\langle d_T \rangle$ for electrons and positrons.

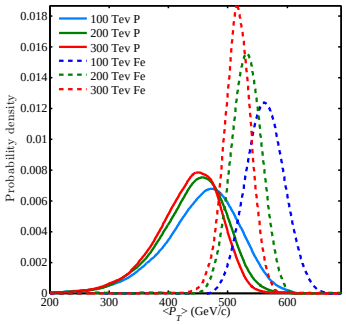

(c) $\langle d_T \rangle$ for muons.

Figure 4: The probability density of $\langle d_T \rangle$. The properties of the applied EASs are shown in the legends.